View metadata, citation and similar papers at core.ac.uk
brought to you by CORE
provided by Repositório Científico do Instituto Politécnico do Porto

Effect of rapid thermal processing conditions on the properties of Cu_2ZnSnS_4 thin films and solar cell performance

M.G. Sousa, A.F. da Cunha, P.A. Fernandes, J.P. Teixeira, R.A. Sousa, J.P. Leitão

A B S T R A C T

In the present work, we have studied the effect of several sulphurization conditions on the properties of Cu_2ZnSnS_4 thin films obtained through rapid thermal processing (RTP) of multi-period precursors with 8 periods of $Zn/SnS_2/CuS$. In this study we varied the heating rate, the maximum sulphurization temperature, the time at maximum temperature and the amount of evaporated sulphur. The samples were characterized through scanning electron microscopy, energy dispersive spectroscopy, Raman scattering spectroscopy, X-ray diffraction, photoluminescence and *I–V* measurements. We have observed that at heating rates above 0.5 °C/s the samples delaminated severely. As a result further tests were carried out at 0.2 °C/s heating rate. The morphological studies revealed that the samples sulphurized at higher temperatures, shorter times and higher amount of evaporated sulphur exhibited larger grain sizes. The structural analysis based on Raman scattering and XRD did not lead to a clear distinction between the samples. Photoluminescence spectroscopy studies showed an asymmetric broad band characteristic of CZTS, which occurs in the range of 1.0–1.4 eV and a second band, on the high energy side of the previous one, peaking at around 1.41 eV. The intensity of this latter band varies from sample to sample revealing substantial differences in their optical properties. This band appears to originate either from the surface of the absorber or from the CdS layer and has a clear correlation with cell efficiency. The higher the intensity of this band the lower the cell efficiency, presumably due to the increase in recombination resulting from CZTS surface decomposition and eventually from the CdS with modified optoelectronic properties. The cell results hint toward a detrimental effect of long sulphurization times and a positive effect of higher sulphur vapour pressure and higher sulphurization temperature. Solar cell efficiencies improved with increased grain size in the absorber layer. The highest cell efficiency obtained in this study was 3.1%.

Keywords:
Kesterites
Cu_2ZnSnS_4
RF-magnetron sputtering
Rapid thermal processing (RTP)

1. Introduction

Cu_2ZnSnS_4 (CZTS) has been an object of intense worldwide research for around half a decade with the main goal of replacing, the more mature, $CuIn_{1-x}Ga_x(Se_{1-y}S_y)_2$ (CIGS) as an absorber layer in thin film solar cells. The advantage of this new compound is that it uses low cost and low toxicity elements [1]. CZTS is a compound whose intrinsic point defects lead to p-type semiconductor behaviour. It presents a direct energy band gap, of approximately 1.5 eV and as a result it shows a high absorption coefficient of $10^4\,cm^{-1}$ [2–4]. These properties confirmed CZTS as a good candidate for replacing CIGS. Available experimental [5] and theoretical [6] results show that the best performances for CZTS based solar cells are obtained with Cu-poor and Zn-rich CZTS. The quality of the CZTS film surface is crucial for the operation of a solar cell. In this respect, it is especially important to try to avoid or minimize CZTS decomposition at the surface. Many methods have been tested to grow this compound but the best results, so far, have been obtained with hydrazine based precursor solutions [7] and coevaporation [8]. Recently, it has been reported the preparation of CZTS by rapid thermal annealing, identical to rapid thermal processing, of electrodeposited elemental precursors leading to films with good crystallinity [9,10]. In this work, the CZTS growth method consists in the sulphurization of precursor layers in a rapid thermal processing furnace. Such a system allows very fast heating rates and very short sulphurization times. We report the results of the characterization of CZTS films, thus obtained, and evaluate their performance in complete solar cells.

The influence of the heating rate, maximum sulphurization temperatures, time at maximum temperatures and the amount of evaporated sulphur during the sulphurization process was studied. A systematic comparison of the influence of the growth conditions on the properties of the CZTS films has been conducted.

2. Experimental methods

In this work, the method used for the growth of CZTS thin films consisted of the rapid thermal processing of multi-period precursor layers. The latter were sequentially deposited by a hybrid RF-magnetron sputtering/evaporation process where SnS_2 and CuS were sputtered whilst Zn was thermally evaporated. All source materials had a purity of 99.999%. The base pressure of the sputtering system was $\sim 10^{-5}$ mbar. The sputtering gas was 90% Ar + 10% H_2, at an operating pressure of 4.0×10^{-3} mbar. This method allowed the deposition of precursors with the following sequence: soda lime glass/Mo/(Zn/SnS_2/CuS) (8 periods). The total thickness of the precursors was 180 nm for Zn, 320 nm for SnS_2 and 660 nm for CuS. The Mo coating of the glass was performed by dc-magnetron sputtering as described by Salomé et al. [11]. The sulphurization was performed in the RTP furnace at an overall pressure of 1 atm consisting of partial pressures of 95% N_2 + 5% H_2 and sulphur vapour resulting from the evaporation of elemental sulphur pieces placed near the sample under treatment. This process was carried out with the samples inside a graphite susceptor covered with a quartz lid and illuminated from the top. In this arrangement it is likely that as the heat treatment proceeds the atmosphere inside the susceptor box becomes sulphur depleted because of its escape and condensation on the cold walls of the furnace chamber. A series of samples was produced in which parameters such as the heating rate, the maximum sulphurization temperature, the time at maximum temperature and the amount of evaporated sulphur were varied. The layers, thus produced, have been finished into complete solar cells by depositing 70 nm thick CdS buffer via chemical bath deposition (CBD) according to a procedure described elsewhere [12] and subsequent deposition of an i-ZnO/ITO window layer via RF-magnetron sputtering. The i-ZnO layer has a thickness of 50 nm and ITO has a thickness of 230 nm. The sheet resistance of the window control sample presented a value of $\sim 50\ \Omega$. The cross-sectional morphology and average composition of the samples were analysed by SEM with a Hitachi Su-70 scanning electron microscope equipped with a Rontec EDS system operated at an acceleration voltage of 4.0 kV for image acquisition and 25 kV for chemical analysis. The crystalline structure was analysed by X-ray diffraction (XRD) with a Philips PW 3710 system, in the Bragg–Brentano configuration (θ–2θ), using the CuKα line (wavelength $\lambda = 1.54060$ Å) and the generator settings were 50 mA and 40 kV. A LabRam Horiba, HR800UV spectrometer, equipped with a solid-state laser oscillating at 532 nm was used for Raman scattering measurements. The photoluminescence (PL) measurements were performed with a Bruker IFS 66v Fourier Transform Infrared (FTIR) spectrometer, equipped with a Ge diode detector, and using 457.9 nm and 514.5 nm lines of an Ar^+ ion laser as an excitation source. A liquid helium flow cryostat was used to vary the temperature of the samples in the range 7–280 K. Ge detector's spectral response correction was performed for all PL spectra. The solar cell performance was characterized through current–voltage (J–V) measurements under simulated standard test conditions in which the light source consisted of a tungsten–halogen lamp combined with an infrared filter for spectrum conditioning. The samples are named according to the maximum sulphurization temperature, time at maximum temperature and the amount of evaporated sulphur. The letters T, t and m, followed by a value, mean the maximum sulphurization temperature, the time at the maximum temperature and the amount of evaporated sulphur, respectively, as described in Table 1.

Table 1
CZTS samples' labelling and summary of the different sulphurization parameters.

Samples	T (°C)	t (min)	m (mg)
T530t2m10	530	2	10
T550t1m10	550	1	10
T530t1m20	530	1	20
T530t2m20	530	2	20
T550t1m20	550	1	20
T550t2m20	550	2	20

3. Results and discussion

The work leading to this paper consisted in the study of how the sulphurization conditions, in a RTP furnace, affect the CZTS properties and the corresponding solar cells' performance. We have observed that at heating rates above 0.5 °C/s the samples delaminated severely. As a result of this, to be on the safe side, further tests were carried out at 0.2 °C/s heating rate. A series of identical precursors was prepared. The results of the compositional analysis, for precursors and CZTS absorber layers after KCN treatment, are shown in Table 2. The EDS analysis showed that the precursors had an excess of Cu and a deficiency of Zn, when compared to those of the Cu-poor and Zn-rich target compositions [5], with a concentration ratio of 1.21 and 1.03 for [Cu]/([Zn + Sn]) and [Zn]/[Sn], respectively. Since the precursors have a layered structure and CuS is their last layer it may happen that Cu is slightly overestimated by EDS. The composition of all the absorber layers, after KCN treatment, is very similar and shows a Sn-rich pattern.

The cross-sectional SEM images of all the samples, after finishing into complete solar cells, are shown in Fig. 1. Here, several comparisons can be made. Comparing samples T530t1m20 with T550t1m20 and T530t2m20 with T550t2m20 we can see that the increase in the maximum sulphurization temperature leads, in both cases, to an increase in grain size. This evidence is more pronounced in the second pair of samples mentioned. More voids are seen in the first pair of samples. Comparing samples T530t1m20 with T530t2m20 and T550t1m20 with T550t2m20 we can see that an increase in the time at the maximum sulphurization temperature leads to a decrease in grain size. This is especially evident for sulphurization at 530 °C. Comparing samples T530t2m10 with T530t2m20 and T550t1m10 with T550t1m20 we can see that an increase in the amount of evaporated sulphur mass at 530 °C does not have a visible effect on the grain size; however at 550 °C it appears that a slight grain growth occurs. The studies reveal that the samples sulphurized at higher temperatures, shorter times and higher amount of evaporated sulphur exhibited larger grains. The crystallinity and phase content of the CZTS films were analysed

Table 2
Composition ratios precursors and CZTS absorber layers, after KCN treatment.

Precursors	$\frac{[Cu]}{[Zn]}$	$\frac{[Cu]}{[Sn]}$	$\frac{[Zn]}{[Sn]}$	$\frac{[Cu]}{[Zn+Sn]}$
	2.40	2.43	1.03	1.21
T530t2m10	1.42	1.51	1.06	0.73
T550t1m10	1.38	1.63	1.18	0.74
T530t2m20	1.59	1.56	0.98	0.79
T530t2m20	1.59	1.46	0.92	0.76
T550t1m20	1.68	1.45	0.86	0.78
T550t2m20	1.62	1.61	0.99	0.81

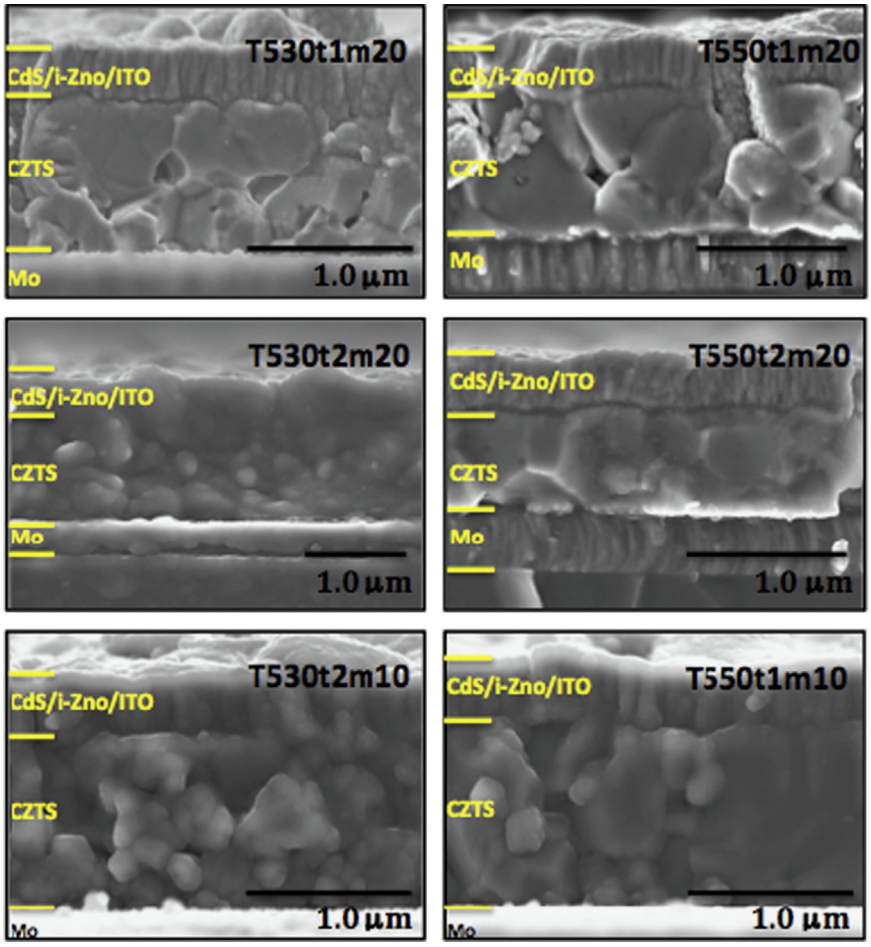

Fig. 1. Cross-sectional SEM micrographs for all the studied samples after being finished into complete solar cells. The cross-sectional morphology of the samples is analysed by SEM with the Hitachi Su-70 scanning electron microscope operated at an acceleration voltage of 4.0 kV.

through Raman scattering. The Raman scattering modes for the crystalline phases that may occur in a CZTS film are shown in Table 3.

The Raman spectra of all the samples are quite similar, as shown in Fig. 2, hence do not provide an insight into the differences in the properties of the layers. CZTS is known to have strong Raman peaks at 288 cm^{-1} and 338 cm^{-1}, which are clearly present, and a less intense peak structure to the right of the main peak between 348 cm^{-1} and 374 cm^{-1}. All the samples showed the structure referred above as a broad shoulder containing components at 348.2 cm^{-1}, 366.8 cm^{-1} and 373.8 cm^{-1} assigned to CZTS. On the left side of the CZTS peak at 288.9 cm^{-1} a broad shoulder extending from 230 cm^{-1} to about 280 cm^{-1} is seen in all the samples; it may have a contribution from the CZTS peak at 252.7 cm^{-1}, CTS peak at 262.4 cm^{-1} and β-ZnS peak at 272.3 cm^{-1}. The main β-ZnS Raman peak occurs at 352.7 cm^{-1} and its identification would require a careful deconvolution of the Raman spectra. Raman scattering structures at 212.1 cm^{-1} and 220.6 cm^{-1} are assigned to SnS_2 and SnS, respectively. This is consistent with the EDS analysis, which shows that the CZTS films are generally Sn-rich. Besides the typical features of CZTS thin films the Raman spectra, discussed above, present a peak at 304 cm^{-1} assigned to the CdS buffer layer.

Since the Raman scattering study does not show a clear distinction between the samples, XRD analysis is performed and two representative diffractograms are shown in Fig. 3. It shows the XRD results for the samples T550t1m20 and T550t2m20. Both diffractograms point to CZTS being the dominant phase present as supported by the presence of several characteristic low intensity CZTS diffraction peaks, which also suggest good crystallinity of the samples. This, however, does not exclude the possibility of there being additional phases such as ZnS and Cu_2SnS_3 (CTS).

Table 3
Raman scattering modes for the crystalline phases that may occur in CZTS films.

Phase	Raman shifts (cm^{-1})	References
Cu_2ZnSnS_4	338, 288, 351, 370	[13–15]
Cu_2SnS_3 (tetragonal)	297, 337, 352	[13]
Cu_2SnS_3 (cubic)	267, 303, 356	[13]
SnS	160, 190, 219	[16–18]
SnS_2	215, 314	[16,19]
Sn_2S_3	52, 60, 237, 254, 307	[16]
ZnS	275–276, 351–352	[13,20]
Cu_2S	475	[13]

In order to acquire a finer understanding of the CZTS properties PL measurements have been performed. Fig. 4(a) shows the normalized PL spectra for all the samples, excited at 457.9 nm and measured at 7 K. Sample T530t2m10 shows only a broad and asymmetric band peaking at ~1.41 eV. The remaining samples exhibit luminescence dominated by a band with maximum at ~1.22 eV, and with a shape clearly asymmetric showing a prominent tail for lower photon energies extending down to ~0.72 eV. For these samples, a shoulder in the high energy side is observed, which seems to correspond to the broad emission observed for sample T530t2m10. As we will discuss later the intensity of this shoulder correlates to solar cell performance. In the case of sample T530t2m10, for which a very weak photovoltaic effect is observed, the emission is dominated by this band. On the other hand, for

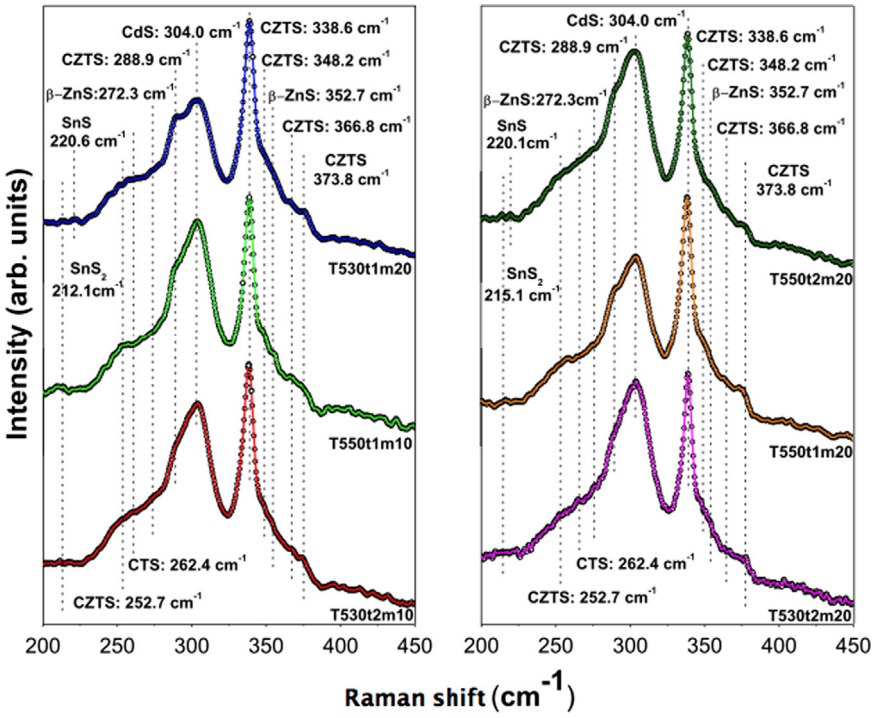

Fig. 2. Raman scattering spectra of all the studied samples. Raman scattering excitation is produced with the solid state laser oscillating at 532 nm.

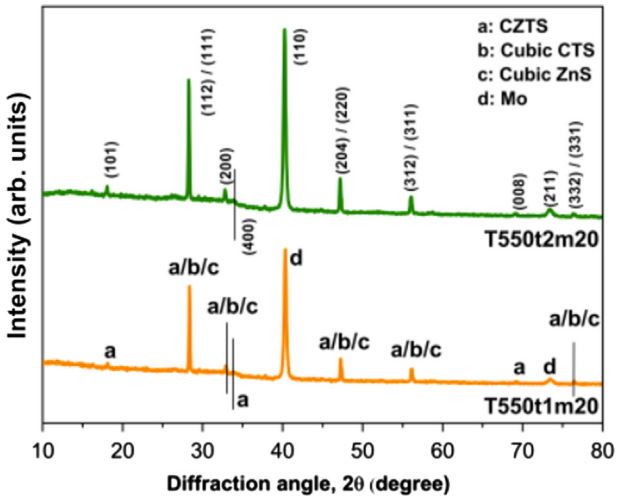

Fig. 3. XRD diffractograms, measured in the Bragg–Brentano configuration (θ–2θ), using the CuKα line (wavelength $\lambda = 1.54060$ Å) and the generator settings are 50 mA and 40 kV, for the samples T550t1m20 (bottom) and T550t2m20 (top), respectively.

sample T550t1m20, the relative intensity of the shoulder is the lowest in the set of samples. As it is evident from the discussion above the PL measurements, unlike the structural analysis, have revealed substantial differences between the CZTS layers, namely regarding the relative intensity of the high energy shoulder.

Fig. 4(b) shows the normalized PL spectra measured at low temperature (7 K) for sample T550t1m20 and for two different excitation wavelengths (457.9 nm and 514.5 nm). We see that the relative intensity of the shoulder in the high energy side increases for the shorter excitation wavelength for which the absorption occurs closer to the top surface of the absorber layer. This result suggests that the origin of the shoulder lies at the interface between CZTS and CdS. This luminescence may be generated within a thin CZTS top layer or in the CdS with properties modelled by CZTS surface. The main asymmetric band originates from deeper inside the absorber layer. A full discussion of the nature of the PL components requires the study of their dependence on the excitation power and temperature, which is underway and will be presented elsewhere.

Fig. 5 shows the solar cells' J–V curves for all the samples studied in order to evaluate their performance. Table 4 shows the solar cells' performance parameters extracted from the J–V curves. Comparing samples T530t1m20 with T550t1m20 and T530t2m20 with T550t2m20 we can see that the increase in the maximum sulphurization temperature, in the first pair, leads to an increase in open circuit voltage (V_{OC}) of about 20 mV and an increase in short circuit current density (J_{SC}) of 4 mA cm^{-2} resulting in a substantial increase in cell efficiency from 2.3% to 3.1%. In the case of the second pair the increase in sulphurization temperature leads to degradation in V_{OC} of about 35 mV and a slight increase in J_{SC} of 1.7 mA cm^{-2} resulting in similar cell efficiencies. Comparing samples T530t1m20 with T530t2m20 and T550t1m20 with T550t2m20 we can see that an increase in the time at the maximum sulphurization temperature leads, in both cases, to a decrease in V_{OC}, J_{SC} and a substantial degradation of the fill factor (FF) resulting in a substantial decrease in the cell efficiency. Comparing samples T530t2m10 with T530t2m20 and T550t1m10 with T550t1m20 we can see that an increase in the evaporated sulphur mass, in the first pair, leads to a dramatic increase in V_{OC} of about 440 mV, in J_{SC} of 8.1 mA cm^{-2} and in FF of 14% which translates, in terms of efficiency, in an increase from a negligible value to 1.6%. In the case of the second pair, an increase in the evaporated sulphur mass leads to an increase in V_{OC} of 44 mV, an increase in J_{SC} of 5.8 mA cm^{-2} and a slight increase in the FF of 1.7% resulting in a substantial increase in cell efficiency from 1.7% to 3.1% which represents the highest efficiency of the set of samples.

The general conclusions drawn from the cell performance analysis are that the increase in the maximum sulphurization temperature leads to an improvement in cell efficiency, the increase in time at the maximum sulphurization temperature degrades the cell efficiency and the increase in the amount of evaporated sulphur improves the cell efficiency. The improvement

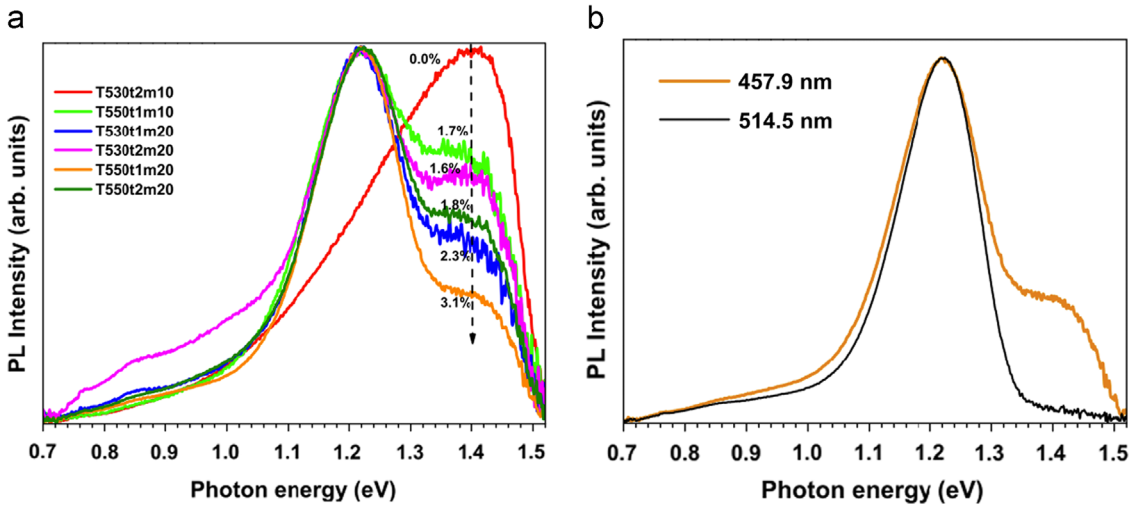

Fig. 4. (a) Normalized PL spectra of all the samples, measured at 7 K with the excitation wavelength of 457.9 nm and the excitation power of 120 mW. (b) Normalized PL for sample T550t1m20 measured at 7 K with two excitation wavelengths: 514.5 nm (black) and 457.9 nm (orange) (excitation power of 100 mW). For interpretation of the references to colour in this figure legend, the reader is referred to the web version of this article.)

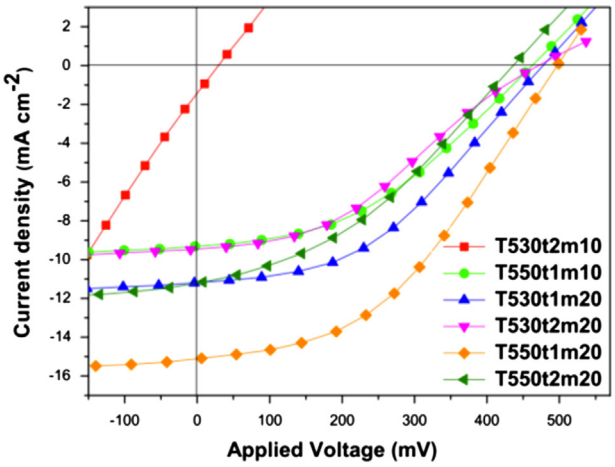

Fig. 5. Solar cell *J–V* curves, acquired under simulated standard test conditions in which the light source consisted of tungsten–halogen lamp combined with the infrared filter for spectrum conditioning, for all the studied samples.

Table 4
Solar cells' performance parameters extracted form *J–V* curves for all the studied samples.

Samples	V_{OC} (mV)	J_{SC} (mA cm^{-2})	FF (%)	Efficiency (%)
T530t2m10	29.4	1.4	22.3	–
T550t1m10	462.4	9.3	40.8	1.7
T530t1m20	476.9	11.2	42.4	2.3
T530t2m20	471.2	9.5	36.3	1.6
T550t1m20	496.7	15.1	42.5	3.1
T550t2m20	435.8	11.2	37.1	1.8

in cell efficiency with increasing maximum sulphurization temperatures occurs alongside the increase in absorber grain size, as shown in Fig. 1. The improvement in cell efficiency may be explained by a reduction in the number of grain boundaries that photogenerated carriers have to cross before being collected at the electrodes, thus undergoing less recombination. The degradation of the cell efficiency with increasing time at maximum sulphurization temperature may be due to CZTS decomposition effects. Besides that, for these samples it is also observed that the absorbers present smaller grains, as shown in Fig. 1. These two factors are known to contribute to increased recombination and thus may explain the reduction in cell efficiency. The improvement in the cell efficiency with increasing amount of evaporated sulphur could be explained by a reduction in the CZTS decomposition. Correlating the cells' performance with the PL measurements it is quite clear that the high intensity of the band at higher energies is associated with a degradation of the cell efficiencies, as shown in Fig. 4. The nature of this relationship is not totally clear but the PL study suggests that this band originates from the top surface of the CZTS absorber or from the CdS layer. If for some RTP conditions decomposition of the CZTS occurs this will influence the CBD growth of CdS and ultimately will influence the properties of this layer. This decomposition is likely to proceed according to the equation given below

$$Cu_2ZnSnS_4(s) \leftrightarrow Cu_2S(s) + ZnS(s) + SnS(g) + (1/n)\ Sn(g) \quad (1)$$

It is known that excess of both sulphur or tin disulphide vapours in the atmosphere, during sulphurization, reduces the CZTS decomposition. The opposite occurs when the atmosphere is deficient in these vapours [21–24].

4. Conclusion

The effects of several sulphurization parameters on the properties of Cu_2ZnSnS_4 thin films obtained through rapid thermal processing (RTP) of multi-period precursor layers were studied. We varied the heating rate, the maximum sulphurization temperature, the time at maximum temperature and the amount of evaporated sulphur. These variations were performed to search for optimum conditions for the crystallization of single phase kesterite thin films. We have observed that at heating rates above 0.5 °C/s the samples delaminated severely. As a result of this further tests were carried out at 0.2 °C/s heating rate. The increase in the maximum sulphurization temperature leads to an increase in grain size. An increase in the time at the maximum sulphurization temperature leads to a decrease in grain size. With an increase in the evaporated sulphur mass a slight grain growth occurs. These studies reveal that the samples sulphurized at higher temperatures, shorter times and higher amount of evaporated sulphur exhibited larger grain sizes. The structural analysis based on Raman scattering and XRD did not reveal clear differences between the CZTS films.

In order to acquire a finer understanding of the CZTS properties PL measurements have been performed and showed an asymmetric broad band, occurring in the range of 1.0–1.4 eV, characteristic of CZTS and a second band, on the high energy side of the previous one, peaking at around 1.41 eV. This latter band appears to originate from the surface of the absorber or from the CdS layer and has a clear correlation with cell efficiency. The higher the intensity of this band the lower the cell efficiency, presumably due to the increase in recombination resulting from CZTS surface decomposition and eventually from the CdS with modified optoelectronic properties. The cell results hint toward the detrimental effect of long sulphurization times and the positive effect of higher sulphur vapour pressure and higher sulphurization temperature, which agrees with earlier reports on decomposition of CZTS at high temperatures in combination with low sulphur pressures. Solar cell efficiencies improved with increased grain size in the absorber layer. The highest cell efficiency obtained in this study was 3.1%.

Acknowledgements

The authors acknowledge the financial support from the Portuguese Science and Technology Foundation (FCT) through Grants PTDC/CTM- MET/113486/2009, PEST-C/CTM/LA0025/2011 and RECI/FIS-NAN/0183/2012.

References

[1] S. Delbos, Kesterite thin films for photovoltaics: a review, EPJ Photovolt. 3 (2012) 35004.
[2] H. Katagiri, M. Nishimura, T. Onozawa, S. Maruyama, M. Fujita, T. Sega, T. Watanabe. Rare-metal free thin film solar cell, in: Proceedings of the IEEE Power Conversion Conference, Nagaoka, Japan, 1997, p. 1003.
[3] P.A. Fernandes, P.M.P. Salomé, A.F. da Cunha, Cu_xSnS_{x+1} (x=2,3) thin films grown by sulfurization of metallic precursors deposited by dc magnetron sputtering, Phys. Status Solidi C 901 (2010) 3–4.
[4] P.M.P. Salomé, J. Malaquias, P.A. Fernandes, M.S. Ferreira, A.F. da Cunha, J.P. Leitão, J.C. González, F.M. Matinaga, Growth and characterization of $Cu_2ZnSn(S,Se)_4$ thin films for solar cells, Sol. Energy Mater. Sol. Cells 101 (2012) 147–153.
[5] H. Katagiri, K. Jimbo, M. Tahara, H. Ariki, K. Oishi, The influence of the composition ratio on CZTS-based thin film solar cells, Mater. Res. Soc. Symp. Proc. (2009) 1165.
[6] S. Chen, A. Walsh, X. Gong, S. Wei, Classification of lattice defects in the kesterite Cu_2ZnSnS_4 and $Cu_2ZnSnSe_4$ earth-abundant solar cell absorbers, Adv. Mater. 25 (2013) 1522–1539.
[7] D.A.R. Barkhouse, O. Gunawan, T. Gokmen, T.K. Todorov, D.B. Mitzi, Device characteristics of a 10.1% hydrazine-processed $Cu_2ZnSn(Se,S)_4$ solar cell, Prog. Photovolt.: Res. Appl. 20 (2012) 6–11.
[8] W. Wang, M.T. Winkler, O. Gunawan, T. Gokmen, T.K. Todorov, Y. Zhu, D.B. Mitzi, Device characteristics of CZTSSe thin-film solar cells with 12.6% efficiency, Adv. Energy Mater. (2013) 1–5.
[9] J. Iljina, R. Zhang, M. Ganchev, T. Raadik, O. Volobujeva, M. Altosaar, R. Trksmaa, E. Mellikov, Formation of Cu_2ZnSnS_4 absorber layers for solar cells by electrodeposition-annealing route, Thin Solid Films 537 (2013) 85–89.
[10] J. Lehner, M. Ganchev, M. Loorits, N. Revathi, T. Raadik, J. Raudoja, M. Grossberg, E. Mellikov, O. Volobujeva, Structural and compositional properties of CZTS thin films formed by rapid thermal annealing of electrodeposited layers, J. Cryst. Growth 380 (2013) 236–240.
[11] P.M.P. Salomé, J. Malaquias, P.A. Fernandes, A.F. da Cunha, Mo bilayer for thin film photovoltaics revisited, J. Phys. D 43 (2010) 345501.
[12] T. Todorov, M. Kita, J. Carda, P. Escribano, Cu_2ZnSnS_4 films deposited by a soft-chemistry method, Thin Solid Films 517 (2009) 2541–2544.
[13] P.A. Fernandes, P.M.P. Salomé, A.F. da Cunha, Study of polycrystalline Cu_2ZnSnS_4 films by Raman scattering, J. Alloys Compd. 509 (2011) 7600–7606.
[14] M. Altosaar, J. Raudoja, K. Timmo, M. Danilson, M. Grossberg, J. Krustok, E. Mellikov, $Cu_2Zn_{1-x}Cd_xSn(Se_{1-y})_4$ solid solutions as absorber materials for solar cells, Phys. Status Solidi A 205 (2008) 167.
[15] W.G Nilsen, Raman spectrum of cubic ZnS, Phys. Rev. 182 (1969) 838–850.
[16] N.R. Mathews, C.C. Garca, I.Z. Torres, Effect of annealing on structural, optical and electrical properties of pulse electrodeposited tin sulphide films, Mater. Sci. Semicond. Process. 16 (2013) 29–37.
[17] L.L. Cheng, M.H. Liu, M.X. Wang, S.C. Wang, G.D. Wang, Q.Y. Zhou, Z.Q. Chen, Preparation of SnS films using solid sources deposited by the PECVD method with controllable film characters, J. Alloys Compd. 545 (2012) 122–129.
[18] G.H. Yue, Y.D. Lin, X. Wen, L.S. Wang, Y.Z. Chen, Synthesis and characterization of the SnS nanowires via chemical vapor deposition, Appl. Phys. A 106 (2012) 87–91.
[19] J. Malaquias, P.A. Fernandes, P.M.P. Salomé, A.F. da Cunha, Assessment of the potential of tin sulphide thin films prepared by sulphurization of metallic precursors as cell absorbers, Thin Solid Films 519 (2011) 7416–7420.
[20] J. Serrano, A. Cantarero, M. Cardona, N. Garro, R. Lauck, R.E. Tall- man, T.M. Ritter, B.A. Weinstein, Raman scattering in β-ZnS, Phys. Rev. B 69 (2004) 014301.
[21] A. Redinger, S. Siebentritt, Coevaporation of Cu_2ZnSnS_4 thin films, Appl. Phys. Lett. 97 (2010) 092111.
[22] A. Weber, R. Mainz, H.W. Schock, On the Sn loss from thin films of the material system Cu–Zn–Sn–S in high vacuum, J. Appl. Phys. 107 (2010) 013516.
[23] J.J. Scragg, T. Ericson, T. Kubart, M. Edoff, C. Platzer-Bjorkman, Chemical insights into the instability of Cu_2ZnSnS_4 films during annealing, Chem. Mater. 23 (2011) 4625–4633.
[24] A. Redinger, D.M. Berg, P.J. Dale, S. Siebentritt, The consequences of kesterite equilibria for efficient solar cells, J. Am. Chem. Soc. 133 (2011) 3320–3323.